



UNIVERSITÀ
DEGLI STUDI
FIRENZE

FLORE

Repository istituzionale dell'Università degli Studi di Firenze

High-temperature oxidation of CrN/AlN multilayer coatings

Questa è la Versione finale referata (Post print/Accepted manuscript) della seguente pubblicazione:

Original Citation:

High-temperature oxidation of CrN/AlN multilayer coatings / U. Bardi; S.P. Chenakin; F. Ghezzi; C. Giolli; A. Goruppa; A. Lavacchi; E. Miorin; C. Pagura; A. Tolstogouzov. - In: APPLIED SURFACE SCIENCE. - ISSN 0169-4332. - STAMPA. - 252:(2005), pp. 1339-1349. [10.1016/j.apsusc.2005.02.105]

Availability:

The webpage <https://hdl.handle.net/2158/775116> of the repository was last updated on

Published version:

DOI: 10.1016/j.apsusc.2005.02.105

Terms of use:

Open Access

La pubblicazione è resa disponibile sotto le norme e i termini della licenza di deposito, secondo quanto stabilito dalla Policy per l'accesso aperto dell'Università degli Studi di Firenze (<https://www.sba.unifi.it/upload/policy-oa-2016-1.pdf>)

Publisher copyright claim:

La data sopra indicata si riferisce all'ultimo aggiornamento della scheda del Repository FloRe - The above-mentioned date refers to the last update of the record in the Institutional Repository FloRe

(Article begins on next page)



High-temperature oxidation of CrN/AlN multilayer coatings[☆]

U. Bardi^{a,b}, S.P. Chenakin^c, F. Ghezzi^d, C. Giolli^{a,b}, A. Goruppa^e,
A. Lavacchi^{a,b}, E. Miorin^f, C. Pagura^f, A. Tolstogouзов^{a,b,*}

^a *Dipartimento di Chimica, Università di Firenze, Via della Lastruccia 3, 50019 Sesto Fiorentino, Italy*

^b *Consorzio Interuniversitario di Scienza e Tecnologia dei Materiali (INSTM) unità di ricerca di Firenze, Via della Lastruccia 3, 50019 Sesto Fiorentino, Italy*

^c *Institute of Metal Physics, National Acad. Sci. of Ukraine, Blvd. Akad. Vernadsky 36, 03680 Kiev-142, Ukraine*

^d *Istituto di Fisica del Plasma (IFP-CNR), Via R. Cozzi 53, 20125 Milano, Italy*

^e *Teer Coatings Ltd, West Stone House, Droitwich, Worcestershire WR9 9AS, UK*

^f *Istituto per l'Energetica e le Interfasi (IENI-CNR), Corso Stati Uniti 4, 35127 Padova, Italy*

Received 25 January 2005; received in revised form 16 February 2005; accepted 16 February 2005

Available online 23 March 2005

Abstract

Experiments are reported on sputter depth profiling of CrN/AlN multilayer abrasive coatings by secondary ion mass spectrometry (SIMS) coupled with sample current measurements (SCM). The coatings were deposited by a closed-field unbalanced magnetron sputtering. It is shown that after oxidation tests, performed in air at 900 °C for 2 h and at 1100 °C for 4 h, the layered structure begins to degrade but is not destroyed completely. Oxidation at 1100 °C for 20 h causes total destruction of the coatings that can be attributed to a fast diffusion of oxygen, nickel, manganese and other elements along defect paths (grain boundaries, dislocations, etc.) in the coating. There are practically no nitrides in the near-surface layer after such a treatment and all the metallic components are in the oxidized form as follows from the data obtained by X-ray photoelectron spectroscopy (XPS). According to XPS and mass-resolved ion scattering spectrometry (MARISS), the surface content of Al in the heat-treated coatings has decreased in comparison with the as-received sample and that of Cr increased. Both XPS and MARISS data exhibit real increase in superficial concentration of the substrate materials (Mn and Ni) that is controversial if using SIMS alone. SCM turned out to be an informative depth profiling method complementary to more expensive and complicated SIMS, being particularly useful for structures with different secondary electron emission properties of the layers. SCM with predetermined SIMS calibration allows a routine characterization of coatings and other multilayer structures, particularly, in situations where the expenses of analysis can be justified.

[☆] Partially presented at the International Workshop on Metal, Metal-Ceramic and Ceramic Protective Coatings, Kiev (Ukraine), 19–23 September 2004.

* Corresponding author. Tel.: +39 055 457 3116; fax: +39 055 457 3120.
E-mail address: alexander.tolstogouзов@unifi.it (A. Tolstogouзов).

© 2005 Elsevier B.V. All rights reserved.

PACS: 68.55.Nq; 82.80.Ms

Keywords: Depth profiling; Mass-resolved ion scattering spectrometry (MARISS); Nitride multilayer coatings; Secondary ion mass spectrometry (SIMS); X-ray photoelectron spectroscopy (XPS); Unbalanced magnetron sputtering

1. Introduction

High-temperature resistant coatings have been developed for a variety of applications. When a considerable hardness is needed, such as for abrasive coatings to be coupled with abradable ones for gap sealing applications, a promising avenue is the fabrication of complex multilayer structures. Amongst them, metallic nitride and oxynitride films [1–6] manufactured by physical vapour deposition (PVD) techniques have proved to be very effective tools due to enhanced mechanical properties (hardness, adhesion, wear, corrosion, and high-temperature resistances).

The optimization of coatings deposition processes and understanding of the degradation mechanisms requires post-growth characterization of the films, usually in terms of chemical composition, phase composition and microstructure by X-ray photoelectron spectroscopy and X-ray diffraction, secondary and transmission electron microscopy, Raman spectroscopy, etc. [7]. Less attention has been paid to the elemental depth profiling in spite of the fact that such measurements enable monitoring interfaces and reveal degradation of the layered structures under different conditions.

This has motivated the present work, aimed at studying the elemental depth profiles of the CrN/AlN multilayer films subjected to high-temperature oxidation in air. The structures were developed by Teer Coatings [8] for application as abrasive coatings for tipping turbine blades. The depth profiling was performed by secondary ion mass spectrometry (SIMS) [9,10] with appropriate calibration of the sputtering rate by a stylus profiler. To obtain complementary information, we simultaneously monitored the variations of ion-induced secondary electron emission via current measurements in the sample circuit. This simple but informative method (for a review, see, e.g. [11–16]) is named “sample-current

measurements” (SCM) [17]. It exhibits high sensitivity to the interlayer boundaries, particularly, for structures with different secondary electron emission properties of the layers and thus allows an integrated depth profiling. In general, variations of secondary electron emission induced by electrons, ions and photons have a long history in characterisation of metal overlayer growth, and a summary of its applications and principles may be found in [18].

X-ray photoelectron spectroscopy (XPS) [19] was employed in our study for surface chemical analysis of the samples, and low-energy ion scattering [20] was enlisted to probe the outer atomic layer of the surface. In contrast to SIMS, the yield of the scattered ions is less sensitive to “matrix effect”. It has been shown [21–25] that complementary mass separation of scattered ions simplifies peak identification and eliminates the overall background related to sputtering of the samples materials that allows avoiding any additional treatment of the spectra. In [21], Wittmaack denoted this technique as mass-resolved ion scattering spectrometry (MARISS) and we used MARISS as an adjuvant method for elemental analysis of the surface.

2. Experimental

The coatings were deposited on a Nimonic-75 superalloy substrate (Ni 75%, Cr 19%, Fe 5%, Mn 1%) using a closed-field unbalanced magnetron sputtering system with opposite Cr and Al targets. Before deposition, the substrate was polished by a diamond paste down to 3 μm and fixed on a cylindrical sample holder in the vacuum chamber ($P = 4.7 \times 10^{-4}$ Pa). It was cleaned by ion bombardment in an Ar plasma discharge ($P_{\text{Ar}} = 0.2$ Pa) and coated in sequence by a bonding Cr layer (ca. 0.3 μm), a transition CrN layer (ca. 0.2 μm) and a gradual introduction of AlN (ca. 0.1 μm). Then, fourteen alternating layers of CrN and AlN with nominal layer widths of 0.3 and 0.1 μm ,

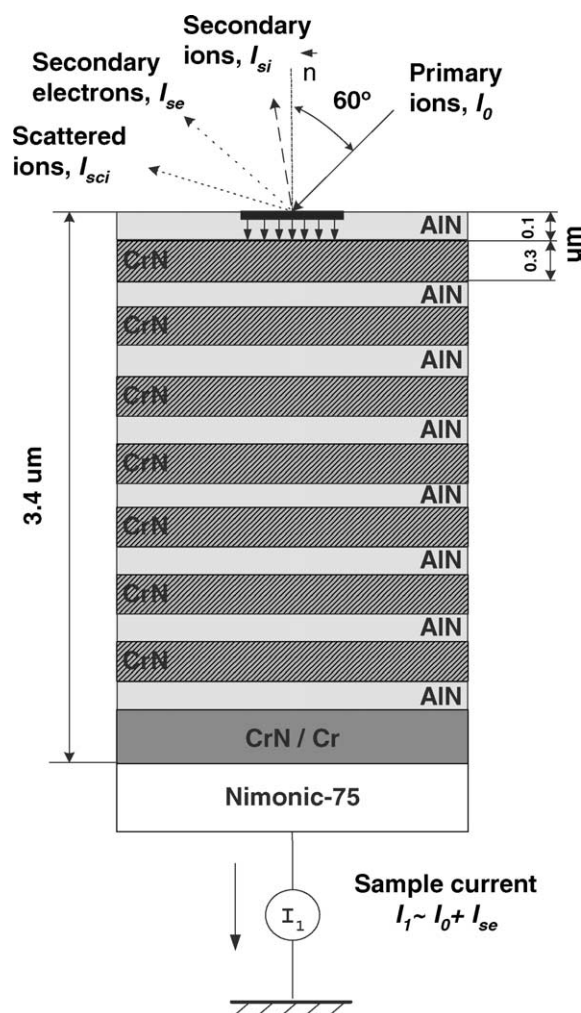


Fig. 1. Cross-section of the sample and schematic view of SIMS–SCM depth profiling arrangement.

respectively, were deposited in a nitrogen flow, which was controlled by an optical emission system with a feedback coupling to a piezoelectric valve. The layer periodicity was adjusted by rotation speed of the sample holder, which was biased by a pulsed DC voltage (250 kHz, –60 V). A schematic cross section of the sample is shown in Fig. 1.

The high-temperature oxidation tests were carried out in a Carbolite furnace (model CWF 13/5) with a maximum operating temperature of 1300 °C and a heating rate of 15 °C/min. Three tests were performed for three as-received samples: 1st, oxidation in the

ambient air at 900 °C for 2 h; 2nd, at 1100 °C for 4 h; and 3rd, at 1100 °C for 20 h.

Secondary ion mass spectrometry and sample current measurements were carried out simultaneously in a high-vacuum (10^{-8} mbar) custom-built installation [23–26] based on standard commercial components. A schematic view of the SIMS–SCM depth profiling arrangement is shown in Fig. 1. A duoplasmatron ion gun (model DP50B by VG Fison) generated mass-filtered $^{16}\text{O}_2^+$ primary ions with a bombarding energy of 3 keV (1.5 keV/atom). The primary ions impinged on the surface at an angle of 60° with respect to the normal. The secondary ions were measured along the normal by a Hiden EQS 1000 Mass Energy Analyser [27], which unifies a high-transmission electrostatic energy analyser and a powerful quadrupole mass spectrometer. The primary beam with an average density of 0.1 mA/cm² was raster-scanned and eroded a sample area of 0.3 mm².

The sample current I_1 was measured in the sample circuit using a free ADC input channel of the Hiden control unit. The value of I_1 is known to be generally determined by the value of the primary ion-beam current I_0 and by the secondary electron emission I_{se} : $I_1 \cong I_0 + I_{se}$, because the currents of secondary ions I_{si} and of scattered ions I_{sci} are rather small as compared with I_{se} . Since I_0 was set in accordance with the ion-gun operation and was kept constant, all variations of I_1 were mostly due to the changes of the secondary electron current I_{se} caused by alteration of the layer properties.

During depth profiling, the intensity of selected secondary ion mass peaks along with SCM data was registered in a quasi-parallel manner under proper apparatus adjustment for each mode. The analysed zone of the crater created by ion bombardment was limited to 10% by means of electronic gating of the registration system for all signals, including sample current. At every instant, we performed two different current measurements: with a positive (+50 V relative to ground) sample potential and a negative (–300 V) potential applied to the surrounding electrodes, and vice versa, i.e. with a negative sample potential and positively biased surroundings. The required secondary electron current I_{se} is calculated as a difference between these measurements.

MARISS measurements were carried out in the same experimental set-up that was used for SIMS–

SCM. A 1 keV Ne^+ beam (without mass separation) was produced by an electron-impact ionisation source IQE 12/38 by SPECS. The incident ions were directed at a fixed incident angle of 30° with respect to the normal. The ions backscattered at the angle $\theta = 120^\circ$ were mass and energy analysed by the Hiden EQS 1000.

XPS analysis was performed in an ultra-high vacuum (10^{-10} mbar) experimental system equipped with a VSW HAC 5000 hemispherical electron energy analyser and an Al $\text{K}\alpha$ X-ray source. Photoelectron spectra were acquired in the constant-pass-energy mode at $E_{\text{pas}} = 44$ eV, and the overall energy resolution was 1.2 eV measured as a full-width at half maximum (FWHM) of the Ag $3d_{5/2}$ line of a pure silver reference. Details of the system have been reported in previous publications [28,29]. The peak positions in XPS were determined by curve fitting after Shirley background subtraction.

During SIMS–SCM, MARISS and XPS analyses of the coatings surface charging effects were negligible despite the AlN film being an insulator. An efficient charge leakage through the coating appears to be associated with metallic-type electrical properties of thick Cr_xN layers [30] or conductivity in the $\text{Cr}_x\text{Al}_{1-x}\text{N}$ structure [31]. In XPS, the binding energies were measured in reference to the C 1s peak of the adventitious aliphatic carbon assumed to be at 284.7 eV.

3. Results and discussion

Fig. 2 shows a mass spectrum of the positively charged secondary ions (in histogram form) measured at the beginning of sputter depth profiling of as-received sample, which has not been exposed to high-temperature oxidation. The spectrum includes different types of secondary ion species and appears very complex. The interpretation of such mass spectra is an intricate problem, especially for quadrupole-based SIMS, which does not provide the same high mass resolution as magnetic and time-of-flight analysers do. Our approach to solving this problem is discussed in detail elsewhere [32] and the results of the mass-spectra decomposition by DECO computer code [33,34] are shown in Table 1. Here, we identified mass peaks of atomic ions of the coating (Al, Cr, N)

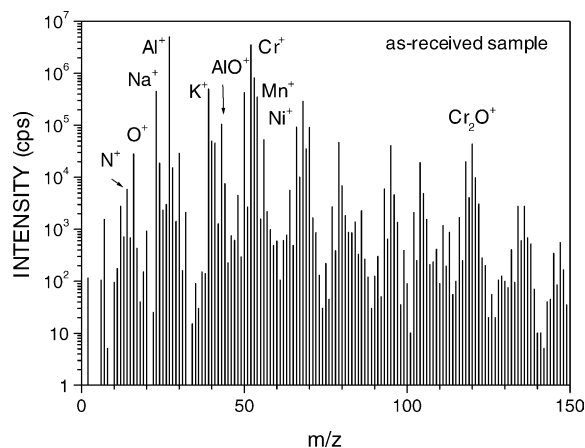


Fig. 2. Mass spectrum of the positive secondary ions measured for the as-received sample.

Table 1

Identification of the main positively charged secondary ions measured for the as-received sample (Fig. 2)

Ion species	Intensity ($\times 10^3$ cps)	Ion species	Intensity ($\times 10^3$ cps)
Al	5020	O ₂	2.1
Cr	4540	CrO ₂	1.7
K	534	Mn	1.6
Na	449	CrAlO ₂	1.5
CrO	345	AlNO	1.3
Al ₂	241	CrOH	1.2
AlO	105	Ni	1.1
CrN	92.2	CrNOH	1.0
Cr ₂ O	65.9	Cr ₂ H	0.9
CrOH ₂	62.4	SiH	0.8
CrAl	57.5	CH	0.7
Ca	51.4	NH	0.7
CrAlO	49.8	CaH	0.3
Fe	40.5		
O	28.3		
Cr ₂	27.4		
Mg	24.0		
Si	16.9		
CaO	16.0		
AlN	9.2		
AlOH	6.5		
N	5.9		
Cr ₂ O ₂	4.5		
Zn	3.2		
C	2.8		
Al ₂ O ₂	2.3		

Sum total of the peak intensities is 1.22×10^7 cps, and the unidentified remainder is 4.2×10^5 cps (3.5%).

and substrate (Ni, Fe, Mn) materials, surface and bulk contaminant species (K, Na, Ca, Mg, Si, Zn, O, C), and different molecular (cluster) ions mainly resulted from oxygen ion-beam irradiation of the sample. The intensities reported in Table 1 are the sum of all isotope ions for every species. The high level of the alkali and alkaline-earth metal ion signals is due to their ultra-high positive ion yields (ionization probability).

We selected $^{14}\text{N}^+$, $^{43}(\text{AlO})^+$ and $^{120}(\text{Cr}_2\text{O})^+$ ions as characteristic masses for depth profiling of the multilayer structure. The substrate material was represented by $^{55}\text{Mn}^+$ and $^{58}\text{Ni}^+$ secondary ions. Atomic $^{27}\text{Al}^+$ and $^{52}\text{Cr}^+$ ions were not monitored in our experiments since the intensity of their emission was very high (more than 4×10^6 cps) and could be distorted due to the saturation of a secondary electron multiplier.

Fig. 3 depicts a three-dimensional image and a cross-section of the sputtered crater for the as-

received sample measured by a Tencor Stylus Profiler P-10. The crater depth Z in the midpoint is about $4\text{ }\mu\text{m}$.

Figs. 4–7 exhibit SIMS and SCM depth profiles of the sample in the initial state and of the samples subjected to high-temperature oxidation. Sputter time is converted into eroded depth by assuming a constant erosion rate $V_{\text{sp}} = Z/T = 13.5 \pm 2.5\text{ nm/min}$, where T is the time of sputtering. The images of the sputter craters measured by an optical microscope are also shown in the panels.

For the as-received sample, the SIMS depth profiles reproduce the expected periodic multilayer structure (Fig. 4a). We estimated the average layer thickness (FWHM) equal to $150 \pm 40\text{ nm}$ for AlN and $280 \pm 40\text{ nm}$ for CrN and layers. These numbers are close to those designed by the manufacturer of the coatings.

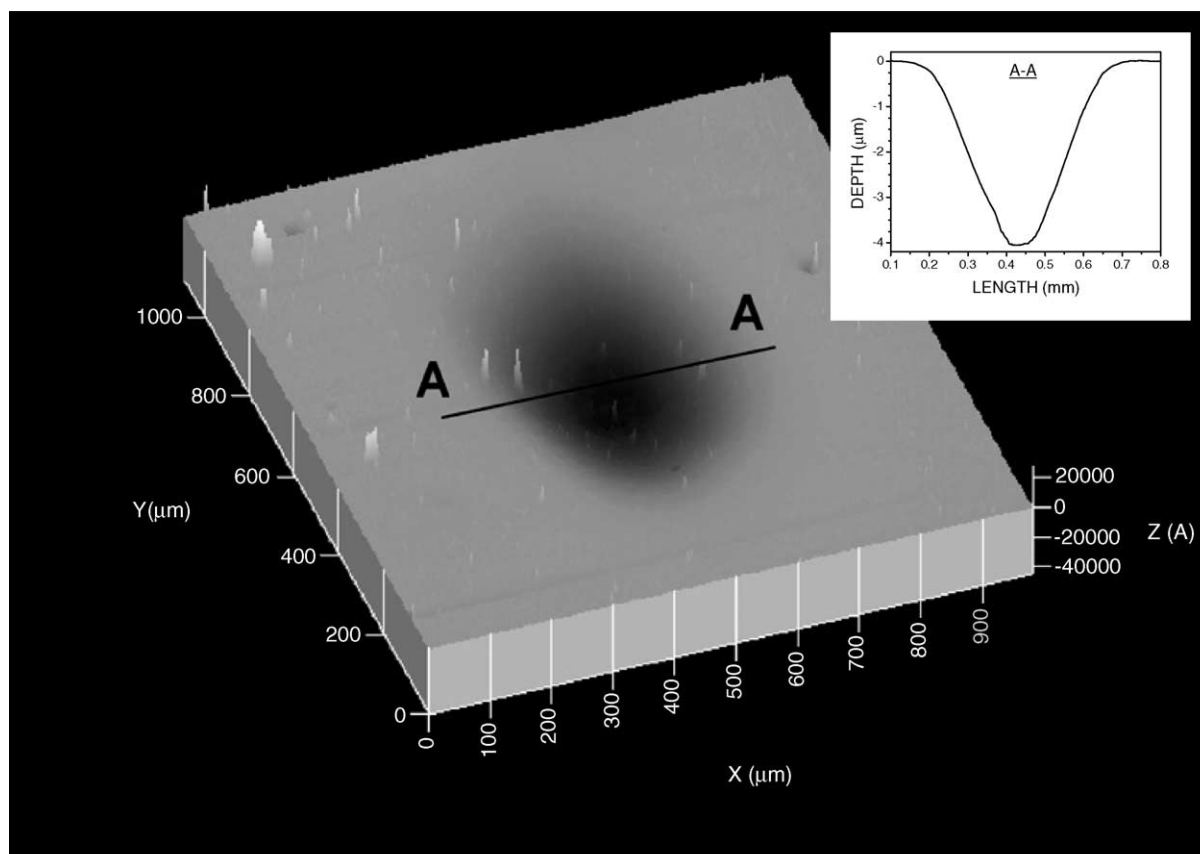


Fig. 3. 3D image of the eroded crater measured by a stylus profiler (inset depicts a cross-section of the crater along the line A-A).

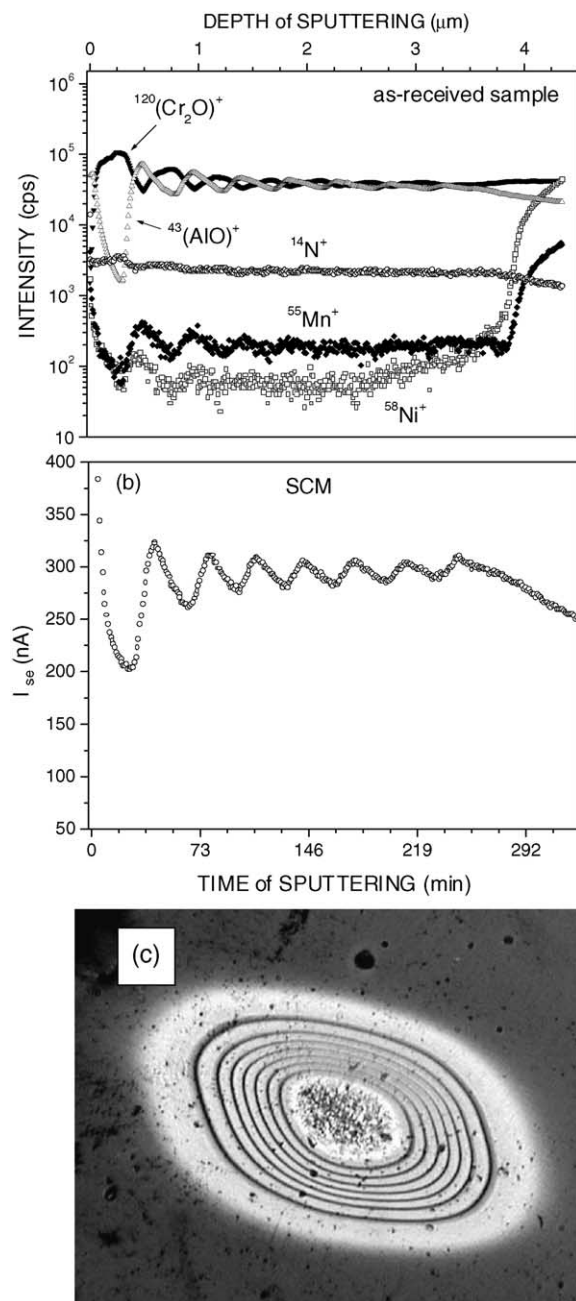


Fig. 4. SIMS (a) and SCM (b) depth profiles, and optical image of the sputter crater (c) for the as-received sample.

All the profiles shown in Figs. 4–7 are disturbed by different artefacts associated with SIMS depth profiling technique. There are well-documented physical and apparatus problems [35,36] that result

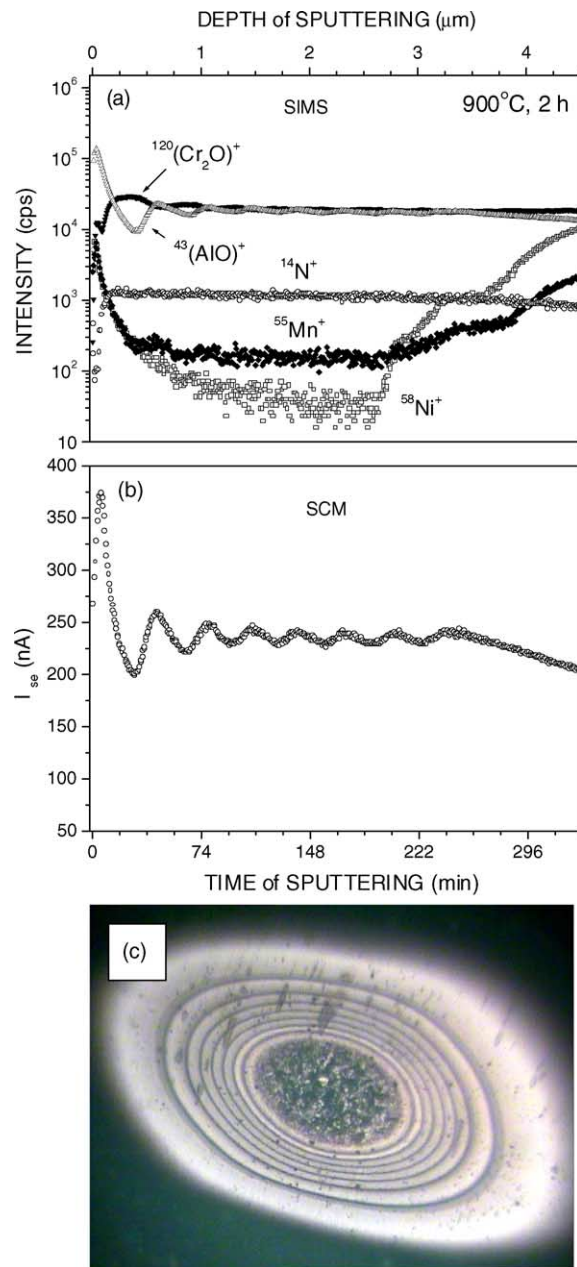


Fig. 5. SIMS (a) and SCM (b) depth profiles, and optical image of the sputter crater (c) for the sample subjected to oxidation in the air at 900 °C for 2 h.

in the loss of depth resolution with increasing eroded depth. We could not totally obviate the disturbances arising from the crater edges, since the overall eroded depth was very large in our experiments. So, it was

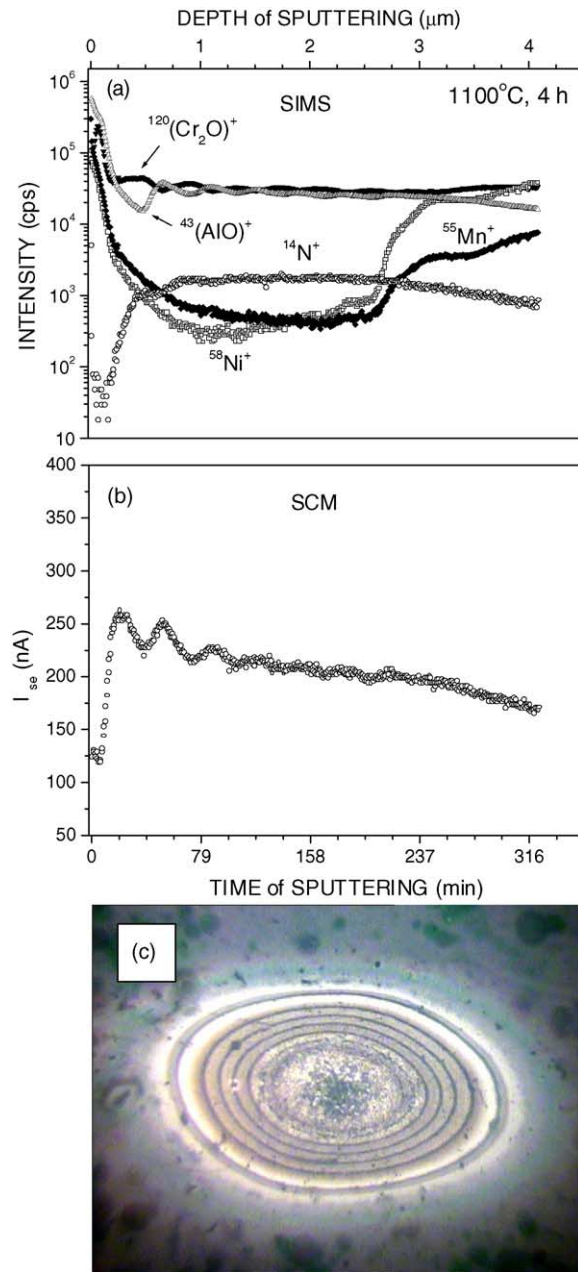


Fig. 6. SIMS (a) and SCM (b) depth profiles, and optical image of the sputter crater (c) for the sample subjected to oxidation at 1100 °C for 4 h.

necessary to decrease the crater size and to increase the bombarding energy in order to hold duration of the analysis in the acceptable limits. Beam-induced interlayer mixing contributes to the degradation of

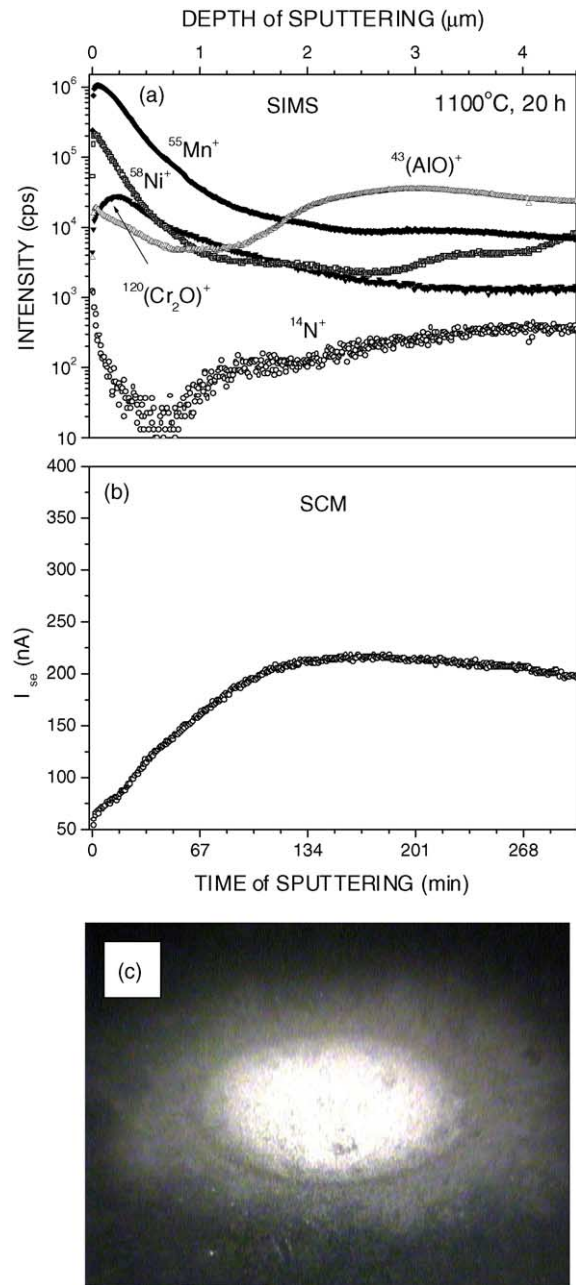


Fig. 7. SIMS (a) and SCM (b) depth profiles, and optical image of the sputter crater (c) for the sample subjected to oxidation at 1100 °C for 20 h.

SIMS profiles as well; it can be considerably suppressed only by lowering the bombarding energy down to 100–200 eV [37] or by using polyatomic or cluster projectiles [38–40]. At present, such techni-

ques are beyond the capabilities of the SIMS instrument used in this study.

The oscillation of the secondary electron current of the as-received sample (Fig. 4b) reproduces the variations of intensity of the AlO^+ secondary ions (Fig. 4a), i.e. I_{se} exhibits sensitivity to elemental composition of the surface revealed under sputter depth profiling. The optical image of the crater (Fig. 4c) shows concentric ellipses related to the multilayer structure, with the bright rings corresponding to Cr-containing layers and the dark ones to Al-containing layers. Since the crater walls are far from vertical (see Fig. 3), the projections of the rings on the crater walls are optically visible (“wedge effect”) despite the fact that original thicknesses of the layers are less than the light wavelength.

XPS analysis of the as-received sample (Fig. 8, curve 1) showed the presence on the surface of Al, Cr, N, O, C, and Na. The surface chemical and phase composition derived from available binding energies of the respective peaks is given in Table 2. The appreciable contamination of the surface of the sample with sodium revealed by XPS is in agreement with SIMS data (see Fig. 2 and Table 1).

The chemical environment for the XPS Al 2p peak cannot be easily distinguished because of the small binding energy (BE) difference between the Al–N and Al–O bonds. However, the availability of the X-ray excited Al KLL Auger peak (Table 2) allows determination of Auger parameter for aluminium in

the compound $\alpha'(\text{Al}) = \text{KE}(\text{Al KLL}) + \text{BE}(\text{Al 2p}) = 1463.7 \text{ eV}$ (here KE stands for the kinetic energy), which is by far more sensitive to the bond type and points out formation of Al–N bonds [41]. The Cr $2p_{3/2}$ peak is dominated by the component ($\text{BE} = 574.8 \text{ eV}$), which can be attributed to nitrogen-deficient chromium nitride close to Cr_2N [42]. There is also a minor component at $\text{BE} = 576.9 \text{ eV}$ indicating formation of chromium oxide/hydroxide on the surface [43]. The nitrogen deficiency in the Cr–Al–N coating may be responsible for a good electrical conductivity [31] preventing from appreciable surface charging during XPS–SIMS analyses. The energy position of the N 1s peak and its satellite at ca. 419 eV (Fig. 8) demonstrate that nitrogen enters into nitrides. According to the results of deconvolution, the O 1s spectrum is composed of three peaks. Two major components located at BEs of 531.7 and 530.2 eV correspond to the signals from oxygen in carbonyl-type species [44] (52% of the total) and in oxide/oxyntiride [31] (39%), respectively, and a minor peak at 535.1 eV can be attributed to adsorbed water [45]. The assignment of the O 1s component at $\text{BE} = 531.7 \text{ eV}$ to carbonyl-type species is consistent with the structure of the asymmetric C 1s spectrum which includes, in addition to the main peak at 284.7 eV (–C–C–bonds), a component at 287.9 eV related to –C=O bonds [44,46] which amounts to about 21% of the total C 1s peak.

MARISS spectra for the as-received sample (curve 1) and for the sample subjected to oxidation at 1100 °C for 20 h (curve 2) are shown in Fig. 9. On the basis of the binary elastic collisions (BEC) model (see, e.g. [20]) we identified the peaks as corresponding to $^{20}\text{Ne}^+$ scattered from Al and Cr atoms (for the as-received sample) and additionally from substrate materials (Mn and Ni) and contaminations (Na, K/Ca) for the heat-treated sample. The narrow peak near-zero energy was caused by Ne^+ ions initially implanted and then re-emitted [21,23]. MARISS is one of the most surface sensitive technique; however, in comparison with SIMS, it is characterized by relatively low elemental sensitivity and small mass resolution. Furthermore, in our backscattering geometry ($\theta = 120^\circ$) the classical laws of conservation of energy and momentum prohibited BEC scattering of a primary ion from a surface atom lighter than the projectile. Hence, we could not monitor by MARISS

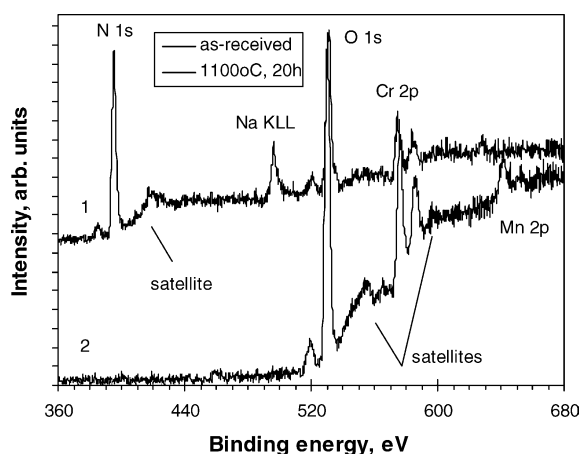


Fig. 8. A selected region of XPS spectra for the as-received sample (1) and for the sample subjected to oxidation at 1100 °C for 20 h (2).

Table 2

XPS data: surface chemical elemental and phase composition of the as-received sample and of the sample subjected to oxidation in air at 1100 °C for 20 h

Element	Line	As-received sample		After high-temperature oxidation	
		BE (eV)	Attribution	BE (eV)	Attribution
Al	Al 2p	72.8	Al–N	73.6	Al–O
	Al KLL	95.7		100.9	
Cr	Cr 2p _{3/2}	574.8	Cr–N [42]	576.1	Cr ₂ O ₃ [52]
		576.9	Cr ₂ O ₃ /Cr(OH) ₃ [43]		
N	N 1s	395.5	Nitrides	–	–
O	O 1s	531.7	–O=C [44]	529.9	O ^{2–} [49]
		530.2	O ^{2–} [50]	531.9	–O=C
		535.1	H–OH [45]	–	–
Mn	Mn 2p _{3/2}	–	–	641.3	MnO, Mn ₃ O ₄ [53]
Ni	Ni 2p _{3/2}	–	–	854.8	NiO [54]
C	C 1s	284.7	–C–C– [44]	284.7	Contamination
		287.9	–C=O [46]		
Na	Na 1s	1071.4	Contamination	–	–

nitrogen, oxygen and other light atoms with masses less than mass of ²⁰Ne⁺ ions.

SIMS, due to its high sensitivity, reveals that substrate components, nickel and manganese, penetrate the whole multilayer coating and segregate at the surface (Fig. 4a), while XPS and MARISS do not detect the presence of these elements on the surface of the as-received sample (Figs. 8 and 9, curve 1). It seems that Ni and Mn, exhibiting high atomic mobility, diffuse readily towards the surface already during the course of the layer deposition.

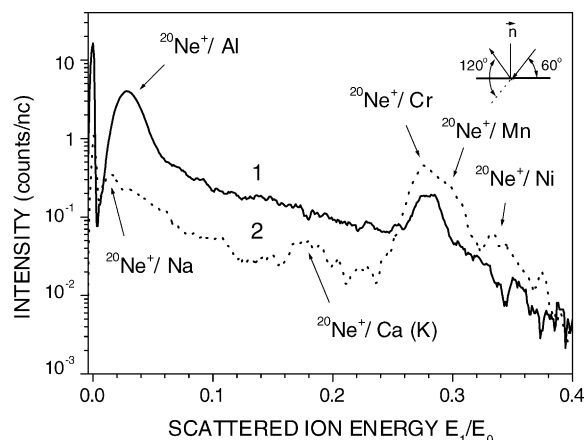


Fig. 9. A selected region of MARISS spectra for the as-received sample (1) and for the sample subjected to oxidation at 1100 °C for 20 h (2).

After the 1st oxidation test (900 °C for 2 h) the layered structure still existed; however, smoothing of the oscillations in the SIMS profiles (Fig. 5a) indicates an enhanced interlayer diffusion. Also, the diffusion of the substrate components (Mn and Ni) towards the surface and the depletion of the subsurface region of nitrogen are clearly observed. At the same time, no significant modifications of the SCM profile and of the optical image of the crater are revealed (Figs. 5b,c), although the amplitude of the SCM oscillations is somewhat decreased.

The second test (1100 °C for 4 h) did not destroy the multilayer structure (Fig. 6a) but it further stimulated interlayer diffusion and strong segregation of Mn and Ni coupled with a drastic decrease in the nitrogen content in the near-surface region. The secondary electron current exhibited damped oscillation with increasing eroded depth (Fig. 6b). The heat treatments at 900 °C for 2 h and 1100 °C for 4 h favoured the process of chemisorption and oxidation induced segregation [47,48] accompanied by a progressive accumulation of Al in the outer layer of the coating and the broadening of the Al-containing layers (Figs. 5a and 6a).

The oxidation performed at the same temperature 1100 °C for 20 h (the third test) resulted in the total elimination of the layered structure, which is evident from both SIMS and SCM profiles shown in Fig. 7a,b. The optical image (Fig. 7c) does not depict any more regular features. The destruction of

the coating structure can be attributed to a fast diffusion of N, O, Ni, Mn and other elements along defect paths (grain boundaries, dislocations, etc.) in both directions, towards the surface and inward the coating.

Accumulation of the substrate components Mn and Ni in the near-surface region of the coating occurring due to strong diffusion of these elements during heat treatment of the sample in the air at 1100 °C for 20 h is clearly demonstrated by respective SIMS depth profiles (Fig. 7a). An intense emission of the Mn^+ and Ni^+ secondary ions is not caused solely by enhancement of respective secondary ion yields due to oxidation but also reflects an appreciable increase in the concentration of these components in the near-surface region which is corroborated by XPS and MARISS analyses of this sample. Indeed, as distinct from as-received sample (Fig. 8, curve 1), a pronounced Mn 2p (Fig. 8, curve 2) and a small Ni 2p peaks are now detected in the spectra. The binding energies of these peaks indicate that they are formed predominantly by photoelectrons emitted from most stable oxides (Table 2).

According to XPS–MARISS data, the surface content of Al in the heat-treated coating has decreased in comparison with the as-received sample and that of Cr increased. After high-temperature oxidation no nitrogen is detected at the surface while oxygen concentration rises significantly (Fig. 8). The main component of the O 1s spectrum at BE = 529.9 eV points out predominant formation of the metal-oxide (O^{2-}) species and seems to be largely associated with Cr_2O_3 [49], though a small contribution of the carbonyl-type bonds is also present. There are practically no nitrides in the surface layer, and all the metallic components in the heat-treated coating are in the oxidized form as follows from their binding energies (Table 2) and as is also indicated by a satellite of the O 1s peak at ca. 555 eV (Fig. 8, curve 2). The emergence of a satellite of the Cr 2p peak at ca. 598 eV (Fig. 8, spectrum 2) provides an evidence of the trivalent state of chromium in oxide [50]. In the oxidized sample, the Al 2p binding energy and Auger parameter for aluminium $\alpha'(\text{Al}) = 1459.3$ eV are somewhat lower than those reported for Al_2O_3 [41,51] that may indicate formation of oxygen-deficient Al_2O_3 or/and of complex Al–Cr–O oxide [51].

4. Summary

The results of the present study provide a detailed characterization of PVD fabricated multilayer CrN/AlN coatings and their resistance to high-temperature oxidation in air. Our focus is on the SIMS–SCM depth profiling of the coatings, which revealed degradation of the layered structure under high-temperature oxidation tests in the air. It was found that heat treatments of the nitride multilayer coating at 900 °C for 2 h and at 1100 °C for 4 h stimulated interlayer diffusion, enhanced segregation of the substrate components (Mn, Ni), brought about a progressive depletion of the near-surface region of nitrogen but did not destroy completely the layered structure. Holding the coating in the air at 1100 °C for 20 h eliminated the layered structure and resulted in the full oxidation of the surface region accompanied by a strong diffusion of the substrate components towards the surface. XPS and MARISS have proved a real increase in superficial concentration of the substrate materials (Mn and Ni) that is controversial, if using SIMS alone. One of the findings of the present work is that the sample current measurements are capable of monitoring interfaces in the multilayer structure as the more complex SIMS technique does. Using SCM with predetermined calibration by SIMS allows a routine characterization of coatings and other multilayer structures, particularly, in situations where the expenses of analysis can be justified.

Acknowledgement

The present work was supported by ABRANEW project RS0098 (FP5 Programme).

References

- [1] P. Verardi, M. Dinescu, C. Gerardi, M. Mirengi, V. Sandu, *Appl. Surf. Sci.* 109–110 (1997) 371.
- [2] C. Emery, A.R. Chourasia, P. Yashar, *J. Electron Spectrosc. Relat. Phenom.* 104 (1999) 312.
- [3] N. Duez, B. Mutel, O. Dessaux, P. Goudmand, J. Grimblot, *Surf. Coat. Technol.* 125 (2000) 79.
- [4] A. Barata, L. Cunha, C. Moura, *Thin Solid Films* 388/389 (2001) 501.

- [5] C. Leyens, M. Peters, P.Eh. Hovsepian, D.B. Lewis, Q. Luo, W.-D. Münz, *Surf. Coat. Technol.* 155 (2002) 103.
- [6] G.S. Kim, S.Y. Lee, J.H. Hahn, S.Y. Lee, *Surf. Coat. Technol.* 171 (2003) 91.
- [7] J.C. Vickerman (Ed.), *Surface Analysis—The Principal Techniques*, Wiley, Chichester, 1997.
- [8] Teer Coatings Ltd, West Stone House, Droitwich, Worcestershire WR9 9AS, UK.
- [9] A. Benninghoven, F.G. Rüdenauer, H.W. Werner, *Secondary Ion Mass Spectrometry*, Wiley, New York, 1989.
- [10] R.G. Wilson, F.A. Stevie, C.W. Magee, *Secondary Ion Mass Spectrometry: A Practical Handbook for Depth Profiling and Bulk Impurity Analysis*, Wiley, New York, 1989.
- [11] P.C. Zalm, L.J. Beckers, *Surf. Sci.* 152/153 (1985) 135.
- [12] A. Tolstogousov, T. Kitaeva, *Pisma v Zhurnal Tekhnicheskoi Fiziki* 20 (1994) 37 (in Russian).
- [13] K. Wittmaack, *Nucl. Instrum. Methods B* 115 (1996) 288.
- [14] K. Wittmaack, *Surf. Sci.* 419 (1999) 249.
- [15] Y. Kataoka, K. Wittmaack, *Surf. Sci.* 424 (1999) 299.
- [16] M.A. Karolewski, *Surf. Sci.* 517 (2002) 138.
- [17] A. Tolstogousov, C.L. Greenwood, *Poverkhnost' (Russ.)* 12 (2002) 33.
- [18] C. Argile, G.E. Rhead, *Surf. Sci. Rep.* 10 (1989) 277.
- [19] B. Ratner, D. Castner, in: J.C. Vickerman (Ed.), *Surface Analysis—The Principal Techniques*, Wiley, Chichester, 1997 p. 43.
- [20] E. Taglauer, in: J.C. Vickerman (Ed.), *Surface Analysis—The Principal Techniques*, Wiley, Chichester, 1997, p. 215.
- [21] K. Wittmaack, *Surf. Sci.* 345 (1996) 110.
- [22] K. Franzreb, A. Pratt, S. Splinter, P.A.W. van der Heide, *Surf. Interface Anal.* 26 (1998) 597.
- [23] A. Tolstogousov, S. Daolio, C. Pagura, *Surf. Sci.* 441 (1999) 213.
- [24] S. Daolio, C. Pagura, A. Tolstogousov, *Appl. Surf. Sci.* 222 (2004) 166.
- [25] A. Tolstogousov, S. Daolio, C. Pagura, *Nucl. Instrum. Methods B* 183 (2001) 116.
- [26] A. Tolstogousov, S. Daolio, C. Pagura, C.L. Greenwood, *Int. J. Mass Spectrom.* 214 (2002) 327.
- [27] Hiden Analytical Ltd, 420 Europe Boulevard, Warrington WA5 7UN, England.
- [28] A. Lavacchi, B. Cortigiani, G. Roviola, U. Bardi, A. Atrei, R. Angelucci, L. Dori, S. Nicoletti, A. Poggi, *Sens. Actuators B* 71 (2000) 123.
- [29] E. Galvanetto, F.P. Galliano, F. Borgioli, U. Bardi, A. Lavacchi, *Thin Solid Films* 384 (2001) 223.
- [30] E. Martinez, R. Sanjinés, O. Banakh, F. Lévy, *Thin Solid Films* 447–448 (2004) 332.
- [31] R. Sanjinés, O. Banakh, C. Rojas, P.E. Schmid, F. Lévy, *Thin Solid Films* 420–421 (2002) 312.
- [32] U. Bardi, S. Caporali, S.P. Chenakin, A. Lavacchi, E. Miorin, C. Pagura, A. Tolstogousov, *Surf. Coat. Technol.*, in press (<http://authors.elsevier.com/sd/article/S0257897204011910>).
- [33] A. Tolstogousov, *Eur. Microsc. Anal.* 3 (1997) 17.
- [34] E. Laptev, unpublished data.
- [35] H.W. Werner, P.R. Boudewijn, in: A.W. Czanderna, T.E. Madey, C.J. Powell (Eds.), *Beam Effects, Surface Topography, and Depth Profiling in Surface Analysis*, Plenum Press, New York, 1998, p. 355.
- [36] S. Hofmann, *Rep. Prog. Phys.* 61 (1998) 827.
- [37] M.G. Dowsett, *Appl. Surf. Sci.* 203–204 (2003) 5.
- [38] G. Gillen, M. Walker, P. Thompson, J. Bennett, *J. Vac. Sci. Technol. B* 18 (2000) 503.
- [39] J. Matsuo, C. Okubo, T. Seki, T. Aoki, N. Toyoda, I. Yamada, *Nucl. Instrum. Methods B* 219–B220 (2004) 463.
- [40] S. Sun, C. Szakal, T. Roll, P. Mazarov, A. Wucher, N. Winoograd, *Surf. Interface Anal.* 36 (2004) 1367.
- [41] J.C. Sánchez-López, M.D. Alcalá, C. Real, A. Fernández, *Nanostruct. Mater.* 11 (1999) 249.
- [42] O. Nishimura, K. Yabe, M. Iwaki, *J. Electron Spectrosc. Relat. Phenom.* 49 (1989) 335.
- [43] F.M. Capece, V. Dicastro, C. Furlani, G. Mattogno, C. Fragale, M. Gargano, M. Rossi, *J. Electron Spectrosc. Relat. Phenom.* 27 (1982) 119.
- [44] T. Belmonte, J.M. Thiébaud, D. Mézerette, *J. Phys. D: Appl. Phys.* 35 (2002) 1919.
- [45] P.D. Schulze, S.L. Shaffer, R.L. Hance, D.L. Utley, *J. Vac. Sci. Technol. A* 1 (1983) 97.
- [46] J. Li, Q. Zhang, S.F. Yoon, J. Ahn, Q. Zhou, S. Wang, D. Yang, Q. Wang, *J. Appl. Phys.* 92 (2002) 6275.
- [47] D. Tománek, S. Mukherjee, V. Kumar, K.H. Bennemann, *Surf. Sci.* 114 (1982) 11.
- [48] S.P. Chenakin, *Metallofizika i Noveishie Tekhnologii* 24 (12) (2002) 1665 (in Russian).
- [49] W.Y. Howng, R.J. Thorn, *J. Chem. Phys. Solids* 41 (1980) 75.
- [50] A.M. Salvi, J.E. Castle, J.F. Watts, E. Desimoni, *Appl. Surf. Sci.* 90 (1995) 333.
- [51] T.L. Barr, *J. Vac. Sci. Technol. A* 9 (1991) 1793.
- [52] G.C. Allen, S.J. Harris, J.A. Jutson, J.M. Dyke, *Appl. Surf. Sci.* 37 (1989) 111.
- [53] B.R. Strohmeyer, D.M. Hercules, *J. Phys. Chem.* 88 (1984) 4922.
- [54] C.P. Li, A. Proctor, D.M. Hercules, *Appl. Spectrosc.* 38 (1984) 880.